RSC Advances

COMMUNICATION

View Article Online
View Journal | View Issue

Cite this: *RSC Adv.*, 2014, **4**, 17141

Synthesis of a meso–macro hierarchical porous carbon material for improvement of O_2 diffusivity in Li–O_2 batteries†

Received 6th March 2014
Accepted 31st March 2014

DOI: 10.1039/c4ra01940g

www.rsc.org/advances

Hongjiao Nie,[ab] Yining Zhang,[a] Jing Li,[ab] Wei Zhou,[ab] Qinzhi Lai,[a] Tao Liu*[a] and Huamin Zhang*[a]

Meso–macro hierarchical porous carbon (HPC) is prepared and used as a cathode material in Li–O_2 batteries. The O_2 diffusivity has been largely improved due to the unblocked macropores. As a result, a better pore utilization and extremely high discharge capacity is achieved.

To meet the demand for higher power density and better energy storage capabilities, much attention has been focused on the development of nonaqueous Li–O_2 batteries.[1–4] With metallic Li anode and O_2 accessed from the environment on a porous cathode, Li–O_2 batteries have the potential to provide a capacity 5–10 times higher than the state-of-art Li-ion cells.[1,4–7] However, the development of Li–O_2 batteries is still in its infancy due to many factors, such as low capacity, poor cycle stability and low energy efficiency, which need significant improvement.[8] To improve the cycle stability and energy efficiency, novel catalyst should be developed. While for high capacity, it is more likely to rely on the optimization of cathode microstructure.

Typical nonaqueous Li–O_2 batteries consist of a lithium metal anode, a separator soaked with organic electrolyte and an air electrode (cathode) in an O_2-filled cell. The oxygen reduction reaction (ORR) of a Li–O_2 battery mainly takes place in the cathode, which is generally porous carbon material. During discharge, Li^+ combines with reduced oxygen to form insoluble lithium oxide (mainly Li_2O_2) at the pore walls of the porous air electrode.[9] Once the pores are completely chocked by these solid products, the discharge process will stop.[10,11] Thus, the microstructure, especially pore structure, of air electrode is a critical factor determining the discharge performance of Li–O_2 batteries.[12] To achieve high discharge capacity, two major factors need to be addressed. First, a large pore volume is requirable, because it could accommodate more discharge products. Second, pore size distribution (PSD) of air electrode is also important, because previous studies have proved that only mesopores with appropriate sizes, *e.g.* tens of nanometers, is favourable to obtain a high utilization.[13,14]

However, it is not to say that larger pore volume at desirable size means higher discharge capacity. Even with applicable sizes, a large proportion of these pores are still unavailable for the deposition of lithium oxide. In a nonaqueous Li–O_2 battery, the reaction takes place at the solid–liquid interface, and O_2 should be dissolved in the electrolyte and diffuses to the interface to participate in the reaction. That is, O_2 should transport through the pores in the air electrode. As the discharge proceeds, the insoluble lithium oxide starts to deposit on air electrode surface. At the very start, the discharge products tend to deposit at the O_2 side with more sufficient gas supply. Once the external pores are chocked, O_2 transmission to the internal sites of electrode will consequently be hindered, which will cause early termination of the discharge process. As a result, the internal pores will be left empty at the end of discharge, just as shown in Fig. 1a, especially in the case of thick

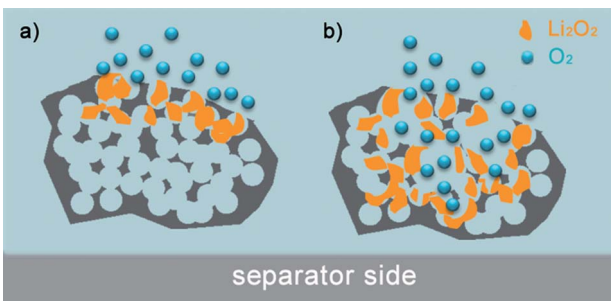

Fig. 1 Schematic representations comparing the distribution of Li_2O_2 for conventional air electrode with only mesopores (a) and air electrode with hierarchical meso–macroporous structure (b).

[a]*Division of Energy Storage, Dalian National Laboratory for Clean Energy, Dalian Institute of Chemical Physics, Chinese Academy of Sciences, Zhongshan Road 457, Dalian, 116023, China. E-mail: zhanghm@dicp.ac.cn; liutao@dicp.ac.cn; Fax: +86-411-84665057; Tel: +86-411-84379072*

[b]*University of Chinese Academy of Sciences, Beijing, 100039, China*

† Electronic supplementary information (ESI) available: Synthesis of HPC and MPC material. Cathode preparations. Material and electrode characterizations. Assembly of Li–O_2 battery cells and discharge performance evaluation. CV test. See DOI: 10.1039/c4ra01940g

electrode, where the mass transport is the dominant factor. The lower diffusion and access capability of O_2 into inside reaction zone become the main constraints limiting battery capacity.[15,16] Much effort has been done to improve the O_2 transportation. One of the alternative routes is to support the active materials on the framework of supporting materials, such as Ni foam and so on, to obtain an efficient O_2 transport. The Li–O_2 battery using such an air electrode demonstrated remarkably enhanced capacity.[17] However, the extra weight of the supporting materials would not be ignored. Overall, the intelligent design of carbon material for improved O_2 transport is still a dilemma for the Li–O_2 battery.

In our opinion, carbon material with hierarchical mesoporous–macroporous structure would be ideal for improvement of O_2 diffusivity in Li–O_2 batteries. During discharge, the mesopores could act as centres for Li_2O_2 crystallization. They deserve maximum use because of their applicable sizes. What is more, for the large macropores, they will remain open after complete discharge to 2 V, which guarantees uninterrupted oxygen flow.[12,18,19] As a result, oxygen can be delivered to the inner regions of the air electrode, thus improving the pore filling ratio with the discharge products and increasing the cell capacity as shown in Fig. 1b.[20] In our previous work, a hierarchical porous carbon containing a small amount of macropores were synthesised and used as cathode material for Li–O_2 battery. The unblocked macropores served as O_2 diffusion channels and the space utilization has been largely enhanced.[13] However, the large macropores mainly unevenly distributed in the interstices among the carbon clusters and the number and size of these macropores were hard to be controlled.

In the present work, a meso–macro dual-pore carbon material for improvement of O_2 diffusivity in Li–O_2 batteries was synthesized through an improved one-step hard template method. By using colloidal silica in two different sizes simultaneously as the hard template, a hierarchical porous structure is expediently constructed. The obtained carbon powder contains numerous mesopores interconnected with large amounts of macropores. And by changing the size of the template, the pore size can be exactly adjusted. Surface morphology and pore structure of carbon powder and the electrodes were analyzed by means of SEM and BET. Cyclic voltammetry (CV) was employed to evaluate the electrochemical activity. Finally, the discharge behaviour of hierarchical porous carbon material was studied in comparison with previous mesoporous carbon material (MPC).

Scanning electron microscopy (SEM) images of as-prepared HPC and MPC powder are shown in Fig. 2a and b. Although both HPC and MPC powder possess spongy structures with disordered open pores, their pore structure are clearly different. There are two different kinds of open pores in both HPC and MPC. One is in the range of tens of nanometers. It originates from the silica particle template *ca.* 20–30 nm. During discharge, the mesopores could act as centres for Li_2O_2 crystallization and they would be fully exploited during discharge owing to their applicable size. The other is macropores at hundreds nanometres range. Predictably, there are much more macropores homogeneously distributed in HPC than that in

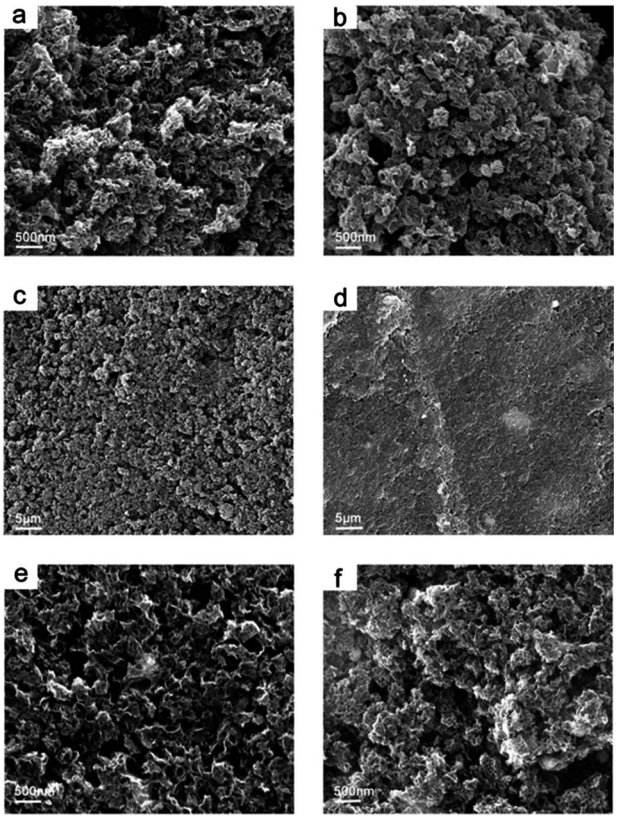

Fig. 2 Scanning electronic microscope (SEM) images of HPC and MPC powder (a and b), HPC and MPC cathode at 5000× (c and d) and 50 000× (e and f).

MPC. It is because that in the fabrication of HPC silica particle of 100–200 nm is added. By template etching, plentiful macropores will be left. In comparison, only small-sized template is employed to synthesize MPC. So only scarce macropores can be found, which mainly come from the interstices among large carbon clusters.

In fact, it is the structure of electrode rather than building material that determines the cell specific capacity. So the morphology of HPC and MPC electrodes were also characterized. Similar to the comparison of building material, the electrodes of HPC and MPC also display quite differently. Fig. 2c and d show that HPC electrode presents an uneven "face", with abundant macropores densely populated throughout the electrode, while MPC electrode appears to be flat and dense. The detailed structures of these electrodes were further confirmed by the magnified SEM images in Fig. 2e and f. HPC electrode is composed of numerous carbon nano-layers. A lot of hundreds of nanometers macropores are surrounded by these carbon nano-layers, making the electrode much looser. Unlike HPC electrode, MPC electrode is constituted by many large aggregates, with few macropores located among them.

The N_2 adsorption/desorption isotherms at 77 K for HPC and MPC are shown in Fig. 3a. Both isotherms are type IV with adsorption hysteresis, indicating the dominant of mesoporosity.[21] The lower and upper parts of the hysteresis loops represent the filling and emptying of the mesopores

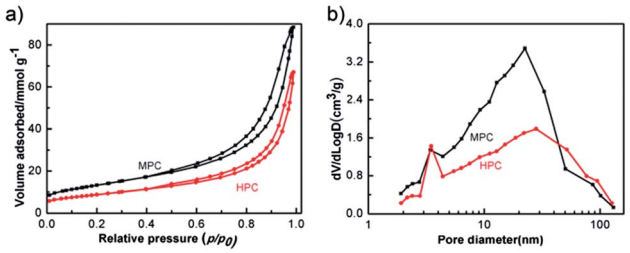

Fig. 3 N_2 adsorption/desorption isotherms (a) and the corresponding pore size distribution curves (b) of HPC and MPC.

respectively.[22,23] In comparison with that of MPC, the amount of gas absorbed by HPC decreases. It means that when large-sized silica particles are added, the porosity for carbon dropped. The decrease in pore volume may be due to the pore collapse caused by the addition of large-sized template. The PSD curves for HPC and MPC are shown in Fig. 3b. Both of them have a similar trend. However, it should be noticed that in the mesopore range, MPC presents a larger pore volume than HPC. It is because that more SiO_2 particles in 20–30 nm were added in MPC. While the macropore volume for HPC obviously increases and exceeds MPC. The large amount of macropores presented in HPC come from the large-sized silica template. It further confirms our observation in Fig. 2.

Since only pores with appropriate sizes (tens of nanometres) could be better used during discharge,[24] all the pores of HPC and MPC are divided into two parts based on their different sizes: pores under 10 nm (pore 1) and pores in the range of 10–100 nm (pore 2). The volume of the two kinds of pores are studied independently and summarized in Table 1. The volume of pore 2 in HPC is 1.46 $cm^3\ g^{-1}$, only 68% that of MPC.

Firstly, the electrochemical activity and kinetic performance of HPC and MPC was evaluated using CV test. CV was first run under argon to provide a background voltammogram. No feature voltammetric currents are observed in the Ar-saturated TEGDME-based electrolyte as shown in Fig. 4a inset, confirming that the electrolyte contains no other electroactive species. Fig. 4a displays the CV curves for the reduction of O_2-saturated electrolyte at a scan rate of 10 mV s^{-1} (background corrected). The reduction peak current (i_p) for HPC is 40% higher than that of MPC, indicating a superior electrocatalytic activity.

Generally speaking, there will be a continuously increasing magnitude of i_p when the scan rate increases. The voltammetric results for HPC and MPC at four different scan rates, 5 mV s^{-1}, 10 mV s^{-1}, 20 mV s^{-1} and 40 mV s^{-1}, are shown in Fig. 4b and c respectively. According to Randles–Sevcik equation (eqn (1))

Table 1 Porosity parameters of HPC and MPC

	S_{BET} ($m^2\ g^{-1}$)	V_t[a] ($cm^3\ g^{-1}$)	V_1[b] ($cm^3\ g^{-1}$)	V_2[b] ($cm^3\ g^{-1}$)
HPC	680	2.09	0.63	1.46
MPC	1064	3.10	0.95	2.15

[a] V_t stands for the total pore volume. [b] V_1, V_2 stand for the volume of pore 1 (under 10 nm) and pore 2 (10–100 nm) respectively.

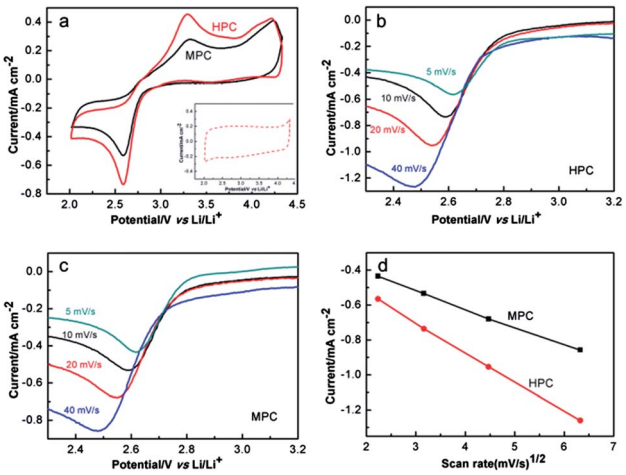

Fig. 4 Cyclic voltammograms for the reduction of O_2-saturated 1.0 M LiTFSI/TEGDME on GC electrode at sweep rate 10 mV s^{-1} (a), the inset shows the corresponding cyclic voltammograms for the reduction of Ar-saturated 1.0 M LiTFSI/TEGDME. Cyclic voltammograms for the reduction of O_2-saturated 1.0 M LiTFSI/TEGDME on GC electrode at sweep rates 5 mV s^{-1}, 10 mV s^{-1}, 20 mV s^{-1} and 40 mV s^{-1} for HPC (b) and MPC (c) respectively. Randles–Sevcik plot of peak current *versus* square root of the scan rate for the curves of HPC and MPC (d).

$$i_p = (2.69 \times 10^5) n^{3/2} A D C V^{1/2} \quad (1)$$

the peak current (i_p) in CV curves is a function of concentration (C), electrode area (A), the number of electrons transferred (n), the diffusion coefficient (D), and the speed at which the potential is scanned (V). The reduction peak currents (i_p) corresponding to various scan rates (V) are collected and a linear relationship between i_p and $V^{1/2}$ is obtained for HPC and MPC (Fig. 4d). It indicates a diffusion controlled electrochemical process.[25] We calculated the diffusion coefficient of O_2 from the dependency of i_p on $V^{1/2}$ (from the Randles–Sevcik equation). The diffusion coefficient for O_2 with HPC cathode is found to be 1.7 times that of MPC cathode. The big difference in the diffusion coefficient values between HPC and MPC implies that the O_2 diffusion coefficient for HPC is remarkably improved owing to its hierarchical meso–macroporous structure.

Discharge tests were then performed to evaluate the cell performance of the two carbon materials. Fig. 5 shows a typical first cycle discharge curves for Li–O_2 batteries at a current density of 30 mA g^{-1}. HPC cathode delivers a dramatically high weight specific capacity of 10 059 mA h g^{-1}, about 2.2 times higher than that of MPC cathode (4480 mA h g^{-1}). Based on the porosity analysis in Table 1, the pore 2 volume of HPC is only 68% that of MPC. It indicates that the space utilization of pore 2 has been efficiently improved when using HPC. Furthermore, considering the different pore volumes of HPC and MPC, the volume specific capacity is also calculated. As shown in Table 2, the volume specific capacity ratio for HPC to MPC increased to 3.3 : 1, further confirming the remarkable enhancement of pore utilization of HPC.

In order to further prove the O_2 transfer improvement in the HPC based air electrode, we disassembled the cells after discharge and studied the lithium oxide distribution under

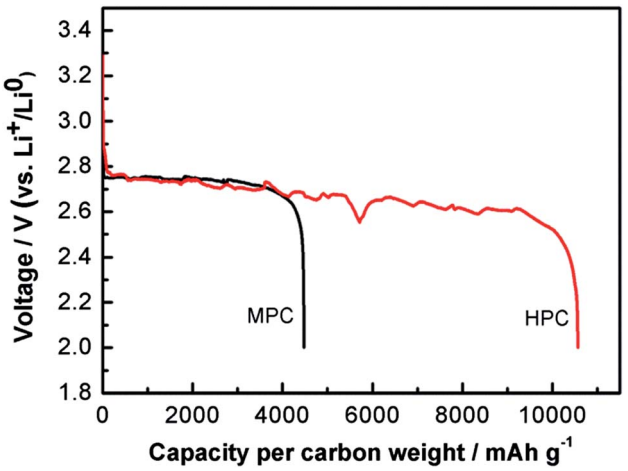

Fig. 5 The first cycle discharge curves of HPC and MPC at 30 mA g^{-1} in 1.2 atm O_2.

Table 2 Specific capacity of HPC and MPC

	Weight specific capacity (mA h g^{-1})	Volume specific capacity (mA h cm^{-3})
HPC	10 059	3884
MPC	4480	1445

SEM. A comparison of the images in Fig. 2 and 6 indicates that the porosity of the electrode decreases significantly after discharge, which can be attributed to the occupation of pores by the reduction products.[26] For MPC electrode, the electrode was covered by a film-like discharge product at the O_2 side, with almost all the pores being filled up (Fig. 6a and b). The resultant discharge product film would block O_2 access to the separator side. As a result, its reduction mainly occurs in the O_2 side, as evidenced by the sparse deposition of electrolyte side in Fig. 6c. With many pores left empty, the use of the inner electrode volume is far below that of the O_2 side, just as shown in the schematic images in Fig. 1a. In comparison, Fig. 6d and e show

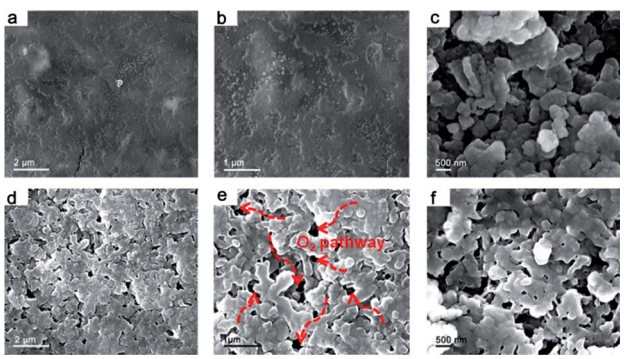

Fig. 6 Morphology of MPC electrode after discharge at the O_2 side (a and b) and separator side (c). Morphology of HPC electrode after discharge at the O_2 side (d and e) and separator side (f), the red arrows in (e) denote the O_2 pathway.

that there still exist a certain amount of open pores at the O_2 side in HPC based electrode, because the large macropores in pristine HPC electrode can not be blocked during discharge due to their large pore size. As a result, it leaves numbers of channels available for the diffusion of O_2. Since gaseous O_2 can easily diffuse all around, the discharge products can be evenly deposited throughout the O_2 electrode (Fig. 1b), resulting in high specific capacity. This is further evidenced by Fig. 6f, which demonstrates a similar Li_2O_2 deposition to Fig. 6e.

Conclusions

In summary, a macro–meso hierarchical porous carbon material was synthesized and used as the cathode material in Li–O_2 batteries. The electrode exhibited an extremely high specific capacity of 10 059 mA h g^{-1}, much higher than the value of 4480 mA h g^{-1} for conventional air-electrode with single pore size. The macropores channels will remain open throughout the discharge process and thus provide uninterrupted oxygen flow to the inner regions of the air electrode, which effectively enhanced the space utilization. As a result, the discharge capacity has been dramatically improved.

Notes and references

1 K. M. Abraham and Z. Jiang, *J. Electrochem. Soc.*, 1996, **143**, 1.
2 P. G. Bruce, *Solid State Ionics*, 2008, **179**, 752.
3 A. Débart, J. Bao, G. Armstrong and P. G. Bruce, *J. Power Sources*, 2007, **174**, 1177.
4 T. Ogasawara, A. Débart, M. Holzapfel, P. Novák and P. G. Bruce, *J. Am. Chem. Soc.*, 2006, **128**, 1390.
5 S. A. Freunberger, Y. Chen, N. E. Drewett, L. J. Hardwick, F. Barde and P. G. Bruce, *Angew. Chem., Int. Ed.*, 2011, **50**, 8609.
6 R. R. Mitchell, B. M. Gallant, C. V. Thompson and Y. Shao-Horn, *Energy Environ. Sci.*, 2011, **4**, 2952.
7 J. Xiao, D. Mei, X. Li, W. Xu, D. Wang, G. L. Graff, W. D. Bennett, Z. Nie, L. V. Saraf, I. A. Aksay, J. Liu and J.-G. Zhang, *Nano Lett.*, 2011, **11**, 5071.
8 R. S. Assary, J. Lu, P. Du, X. Luo, X. Zhang, Y. Ren, L. A. Curtiss and K. Amine, *ChemSusChem*, 2013, **6**, 51.
9 A. Débart, A. J. Paterson, J. Bao and P. G. Bruce, *Angew. Chem., Int. Ed.*, 2008, **47**, 4521.
10 M. Mirzaeian and P. J. Hall, *J. Power Sources*, 2010, **195**, 6817.
11 J. Read, *J. Electrochem. Soc.*, 2006, **153**, A96.
12 V. Etacheri, D. Sharon, A. Garsuch, M. Afri, A. A. Frimer and D. Aurbach, *J. Mater. Chem. A*, 2013, **1**, 5021.
13 H. Nie, H. Zhang, Y. Zhang, T. Liu, J. Li and Q. Lai, *Nanoscale*, 2013, **5**, 8484.
14 X.-h. Yang, P. He and Y.-y. Xia, *Electrochem. Commun.*, 2009, **11**, 1127.
15 J. Read, K. Mutolo, M. Ervin, W. Behl, J. Wolfenstine, A. Driedger and D. Foster, *J. Electrochem. Soc.*, 2003, **150**, A1351.
16 S. S. Zhang, D. Foster and J. Read, *J. Power Sources*, 2010, **195**, 1235.

17 S. D. Beattie, D. M. Manolescu and S. L. Blair, *J. Electrochem. Soc.*, 2009, **156**, A44.
18 J. Li, H. Zhang, Y. Zhang, M. Wang, F. Zhang and H. Nie, *Nanoscale*, 2013, **5**, 4647.
19 Y. Zhang, H. Zhang, J. Li, M. Wang, H. Nie and F. Zhang, *J. Power Sources*, 2013, **240**, 390.
20 R. E. Williford and J.-G. Zhang, *J. Power Sources*, 2009, **194**, 1164.
21 Y. a. Huang, S. Hu, S. Zuo, Z. Xu, C. Han and J. Shen, *J. Mater. Chem.*, 2009, **19**, 7759.
22 Y. Gao, C. Wang, W. Pu, Z. Liu, C. Deng, P. Zhang and Z. Mao, *Int. J. Hydrogen Energy*, 2012, **37**, 12725.
23 C. Tran, J. Kafle, X.-Q. Yang and D. Qu, *Carbon*, 2011, **49**, 1266.
24 C. Tran, X.-Q. Yang and D. Qu, *J. Power Sources*, 2010, **195**, 2057.
25 C. O. Laoire, S. Mukerjee and K. M. Abraham, *J. Phys. Chem. C*, 2009, **113**, 20127.
26 J. Xiao, D. Wang, W. Xu, D. Wang, R. E. Williford, J. Liu and J.-G. Zhang, *J. Electrochem. Soc.*, 2010, **157**, A487.